**NURETH14-167** 

# CFD AIDED DESIGN OF THE EXPERIMENTAL HELIUM LOOP FOR VHTR SIMULATION

Churl Yoon, Sung Deok Hong, Jae Man Noh, Yong Wan Kim and Jong Hwa Chang Korea Atomic Energy Research Institute, Daejeon, Korea <a href="mailto:cyoon@kaeri.re.kr">cyoon@kaeri.re.kr</a>, <a href="mailto:sdhong1@kaeri.re.kr">sdhong1@kaeri.re.kr</a>, <a href="mailto:jmnoh@kaeri.re.kr">jmnoh@kaeri.re.kr</a>, <a href="mailto:ywkim@kaeri.re.kr">ywkim@kaeri.re.kr</a>, <a href="mailto:jhchang@kaeri.re.kr">jhchang@kaeri.re.kr</a>

#### **Abstract**

A medium-scale helium loop for simulating a VHTR (Very High Temperature Reactor) is now under construction in KAERI (Korea Atomic Energy Research Institute). Two electric heaters of the test helium loop heat the helium fluid up to 950°C at a pressure of 1 ~ 9MPa. To optimize the design specifications of the experimental helium loop, conjugate heat transfer in the hightemperature helium heater was analyzed by using CFD (Computational Fluid Dynamics) simulation. The main factors tested in this CFD analysis were the effects of turbulence, radiation, gravity, and geometrical configuration of the heater. From the analysis results, the optimum design configuration was selected confirming that thermal characteristics of the heater well meet the design requirements. In this study, the interrelated effects of buoyancy forces and radiation heat transfer on the geometrical configuration were closely investigated. It was concluded that the buoyancy effects on the helium flows of the heater would be suppressed by the radiation heat transfer inside the heating channel. Various emissivity values of the reflector material emissivity were also tested. Gravity had greater effects on the temperature distribution for the lower emissivity, but the maximum temperature variations due to the emissivity changes from 0.1 to 0.9 were limited to within a few tens of degrees. Finally, more detailed analyses on the HTH of the medium scale helium loop including the spacers were performed and it is confirmed that the thermal-fluidic characteristics of the HTH satisfied the design requirements.

### Introduction

A VHTR is a nuclear power generation system using helium gas and graphite as a coolant and moderator, respectively. This reactor has been selected as one of the next-generation nuclear reactors due to its high coolant outlet temperature of up to 950°C, high efficiency in energy conversion, and safer characteristics due to the low power density. In particular, the high temperature of the primary loop coolant outlet enables the utilization of a VHTR for hydrogen production or industrial processes. [1, 2]

In KAERI, a small size nitrogen loop was constructed in 2008, and is being operated for the tests of a 10kW PHE (Process Heat Exchanger) and the components and materials of a hydrogen production module. [3, 4] Another medium-scale helium loop is under construction [5], the main purposes of which are to support the design and verification of various VHTR and HPM (hydrogen production module) components and to develop experimental technology for a VHTR.

The key components of the primary loop of the medium scale facility such as a circulator and heat exchangers were manufactured in 2009. The primary loop for simulating a VHTR was assembled in 2010. In the year of 2011, the second loop for simulating a HPM will be assembled and the tests of a 150kW PHE and the high-temperature materials and components for a VHTR will be started.

For the high temperature heater of a medium-scale helium loop, a number of thermal-fluidic design requirements exist along with the mechanical requirements such as flow induced vibration, acoustic vibration, and thermal stress. Table 1 summarizes these thermal-fluidic design requirements. The purposes of this study are to optimize the design specifications of the high temperature heater of the experimental helium loop and to examine whether a candidate design meets the thermal-fluidic design requirements using CFD simulation. For these purposes, CFD analyses were performed with simple models and coarse meshes on simplified heater geometry firstly and then gravity and emissivity effects were analysed on the thermal-fluidic behaviour inside the heating channel where helium passes through, and finally the smaller interested region of the high temperature heater was simulated with finer meshes on a more detailed geometry.

# 1. Analysis Methodology

In the first stage, preliminary CFD analyses were performed on a simple straight helium heater ignoring the flow irregularities at the inlet and the outlet as well as by the spacers. At this stage, gravitational effect was not accounted for, and the emissivity of the heater surface was assumed as 0.8. At the later stage, more sophisticated modelling and complex geometry has been added to the investigation.

Figure 1 shows the schematics of the medium scale helium loop which consists of three separated loop. The first loop represents the VHTR primary heat transfer system, while the second and the third stand for the hydrogen production module and a cooling loop, respectively. The first loop of the medium scale helium loop has two helium heaters in series to heat coolant up to high temperature. The first and second loops have a nitrogen supplier as well as a helium one in order for a trial run.

## 1.1 Models and Governing Equations

The continuity, momentum, and energy equations were solved using a commercial CFD code, ANSYS CFX release 13.1.

$$\frac{\partial \rho}{\partial t} + \frac{\partial \left(\rho u_j\right)}{\partial x_j} = 0 \tag{1}$$

$$\frac{\partial (\rho u_i)}{\partial t} + \frac{\partial (\rho u_j u_i)}{\partial x_j} = -\frac{\partial p}{\partial x_i} + \frac{\partial}{\partial x_j} \left[ \mu_e \left( \frac{\partial u_i}{\partial x_j} + \frac{\partial u_j}{\partial x_i} \right) \right] + S$$
 (2)

The 14<sup>th</sup> International Topical Meeting on Nuclear Reactor Thermalhydraulics, NURETH-14 Toronto, Ontario, Canada, September 25-30, 2011

$$\frac{\partial(\rho H)}{\partial t} + \frac{\partial(\rho u_j H)}{\partial x_j} = \frac{\partial}{\partial x_j} \left( \Gamma_e \frac{\partial H}{\partial x_j} \right) + Q \tag{3}$$

Here, the effective viscosity  $\mu_e = \mu + \mu_t$  with  $\mu_t =$  eddy viscosity. In the standard k- $\varepsilon$  turbulence model where the eddy viscosity is defined as  $\mu_t = \rho C_\mu \frac{k^2}{\varepsilon}$ , the transport equations of turbulent kinetic energy (k) and turbulent dissipation rate  $(\varepsilon)$  becomes,

$$\frac{\partial(\rho k)}{\partial t} + \frac{\partial(\rho u_j k)}{\partial x_j} = \frac{\partial}{\partial x_j} \left[ \left( \mu + \frac{\mu_t}{\sigma_k} \right) \frac{\partial k}{\partial x_j} \right] + P_k - \rho \varepsilon + P_{kb}$$
(4)

$$\frac{\partial(\rho\varepsilon)}{\partial t} + \frac{\partial(\rho u_{j}\varepsilon)}{\partial x_{j}} = \frac{\partial}{\partial x_{j}} \left[ \left( \mu + \frac{\mu_{t}}{\sigma_{\varepsilon}} \right) \frac{\partial\varepsilon}{\partial x_{j}} \right] + C_{1}P_{k} \frac{\varepsilon}{k} - C_{2}\rho \frac{\varepsilon^{2}}{k} + C_{1}P_{\varepsilon b} \frac{\varepsilon}{k}$$
(5)

Here, the contants  $C_1$ ,  $C_2$ ,  $\sigma_k$ ,  $\sigma_{\varepsilon}$ , and  $C_{\mu}$  are 1.44, 1.92, 1.0, 1.3, and 0.09, respectively.  $P_k$  is the turbulence production due to viscous forces, and  $P_{kb}$  and  $P_{\varepsilon b}$  represent the influence of the buoyancy forces. If the standard k- $\omega$  turbulence model is adopted, equation (4) and (5) will be replaced with the transport equations of turbulent kinetic energy (k) and specific dissipation rate ( $\omega$ ) associated with a new definition of the eddy viscosity of  $\mu_t = \rho \frac{k}{\omega}$ .

$$\frac{\partial(\rho k)}{\partial t} + \frac{\partial(\rho u_j k)}{\partial x_j} = \frac{\partial}{\partial x_j} \left[ \left( \mu + \frac{\mu_t}{\sigma_k} \right) \frac{\partial k}{\partial x_j} \right] + P_k - \beta \rho k \omega + P_{kb}$$
 (6)

$$\frac{\partial(\rho\omega)}{\partial t} + \frac{\partial(\rho u_j\omega)}{\partial x_j} = \frac{\partial}{\partial x_j} \left[ \left( \mu + \frac{\mu_t}{\sigma_\omega} \right) \frac{\partial\omega}{\partial x_j} \right] + \alpha \frac{\omega}{k} P_k - \beta \rho \omega^2 + P_{\omega b}$$
 (7)

Here, the constants  $\beta$ ',  $\alpha$ ,  $\beta$ ,  $\sigma_k$ , and  $\sigma_{\varepsilon}$  are 0.09, 5/9, 0.075, 2 and 2, respectively.  $P_{\omega b}$  represent the influence of the buoyancy forces. To properly predict the onset and amount of flow separation from smooth surfaces, the shear-stress transport (SST) k- $\omega$  turbulence model can be used by multiplying a limiter to the eddy viscosity in the above equation set. [6]

Because the boundary conditions of the turbulent parameters are not fully specified at the wall, the above turbulence models need a proper wall treatment to provide near-wall boundary conditions for the mean flow and turbulence transport equations. In the standard k- $\varepsilon$  turbulence model, the near-wall mesh node is assumed to be in the log-law region and the minimum value of  $y^+$  is set to be 11.06. In the k- $\omega$  based turbulence model, the near-wall mesh node is assumed to be in the sub-layer region and a fine grid with  $y^+$  around 1 is recommended.

$$y^{+} = \frac{\rho \Delta y u_{\tau}}{\mu}$$
, with  $u_{\tau} = \left(\frac{\tau_{w}}{\rho}\right)^{1/2}$  (8)

Due to the high temperature difference between the heater walls and the inner surface of the reflector and between the vessel outer surface and environment, radiation heat transfer should be accounted for in computation to obtain a realistic solution. The spectral radiative transfer equation can be written as follows, assuming that the scattering is isotropic.

$$\frac{dI_{\nu}}{ds} = -\left(K_{a\nu} + K_{s\nu}\right)I_{\nu} + K_{a\nu}I_{b} + \frac{K_{s\nu}}{4\pi} \int_{4\pi} I_{\nu} \Phi_{\nu} \left(\vec{s} \cdot \vec{s}'\right) d\Omega' + S \tag{9}$$

Here,  $I_v$  is spectral radiation intensity which depends on position  $(\vec{r})$  and direction  $(\vec{s})$ .  $I_b$  is Blackbody emission intensity and can be evaluated as  $I_b = \frac{\sigma n^2 T^4}{\pi}$  with  $\sigma = \text{Stefan-Boltzmann}$ 

constant and n = refractive index.  $K_{a\nu}$  and  $K_{s\nu}$  are the spectral absorption and scattering coefficients. If the discrete transfer (DT) radiation model is adopted, the main assumption is that the radiation leaving a surface element in a certain range of solid angles can be approximated by a single ray. The solution for the intensity  $I_{\nu}$  along rays leaving from the boundaries can be estimated from the equation of radiation transfer by assuming that the system is reasonably homogeneous and that the refractive index is unity.

$$I_{\nu}(s) = I_{\nu 0} \exp(-(K_{a\nu} + K_{s\nu})s) + \frac{\sigma T^{4}}{\pi} (1 - \exp(K_{a}s)) + K_{s\nu} \overline{I}_{\nu}$$
(10)

In this study, a P-I radiation heat transfer model was also adopted, in which all the radiation intensity is isotropic at a given location in space. When we define the spectral incidence radiation as  $G_{\nu} \equiv \int I_{\nu} d\Omega$ , the spectral radiative heat flux can be computed as follows without detailed derivation [7].

$$q_{rv} = -\frac{1}{3(K_{av} - K_{sv}) - AK_{sv}} \nabla G_v \tag{11}$$

Here, A is the linear anisotropy coefficient. The spectral radiative heat flux,  $q_{\nu}$ , passing through a surface at some location  $\vec{r}$  with a unit vector  $\vec{n}$  is defined by

$$q_{rv} = \int (\vec{s} \cdot \vec{n}) I_{v}(\vec{r}, \vec{s}) d\Omega_{s}.$$

Integrating the equation of transfer over solid angles with the assumptions that all the surfaces were diffuse and grey, one can get

$$-\nabla q_r = K_a G - 4K_a \sigma T^4 + S \tag{12}$$

Hence, combining equation (11) and (12) gives

$$\nabla(\Gamma \nabla G) - K_a G + 4K_a \sigma T^4 = S , \text{ with } \Gamma = \frac{1}{3(K_a - K_s) - AK_s}$$
(13)

Table 1 Thermal-fluidic design requirements for the high temperature heater of a mediumscale helium loop

Parameter	Design Requirements			
Internal Insulator	<ul> <li>Operating T &gt; 1500 °C</li> <li>Thickness (Kaowool) &gt; 27 mm</li> </ul>			
Vessel internal	<ul> <li>Heater outlet T &gt; 950 °C</li> <li>Heater max. T &lt; 1600 °C</li> <li>Reynolds number &gt; 2300</li> <li>Liner Reflection</li> </ul>			
Vessel	- Outer surface T < 350 °C			

Equation (13) is the transport equation for G, and equation (12)can be directly substituted into the energy equation to account for heat sources due to radiation.

The governing equations are discretized by using an element-based finite volume method. The advection terms are treated with the high resolution scheme. To accelerate converging speed for the interrelated energy and momentum equation systems, the solution set of (u, v, w, p) are solved coincidently as one matrix for the coupled-solver algorithm. [6]

#### 1.2 Boundary Conditions and Sources

Under normal operating conditions, the total heat load and helium mass flow rate are 270 kW and 0.1 kg/s, respectively. The heat generation rates of the electric heaters were set to be uniform assuming homogeneous material composition and constant cross-sectional areas along the axis. The inlet fluid temperature formerly heated in the low-temperature heater is 500°C. Since the temperature of the outer surface goes up to a few hundred degrees celcius, the boundary condition at the outer wall surface including radiation heat transfer becomes the following.

$$q_{w}'' = h(T_{w} - T_{\infty}) + F\varepsilon\sigma(T_{w}^{4} - T_{\infty}^{4})$$

$$= \left\{ h + F\varepsilon\sigma(T_{w}^{2} + T_{\infty}^{2})(T_{w} + T_{\infty}) \right\} (T_{w} - T_{\infty})$$
(14)

Here the heat transfer coefficient h is assumed to be a constant value of 10.0 W/m<sup>2</sup>K, which is estimated from the empirical correlation for the natural convection around a vertical/horizontal cylinder. The view factor F reaches unity. The emissivity  $\varepsilon$  of the vessel outer surface is assumed to be 0.8, which is obtained from a emissivity value of oxidized steel. The Stefan-Boltzmann constant  $\sigma$  is 5.6704x10-8 W/m<sup>2</sup>K<sup>4</sup>. In computation, the energy boundary condition at the outer surface of the pipe was implemented explicitly. That is, the heat fluxes obtained from equation (14) were treated as a source term of the energy equation by substituting the calculated surface temperature at the previous time step,  $T_{\rm w}^{\rm old}$ , into  $T_{\rm w}$ .

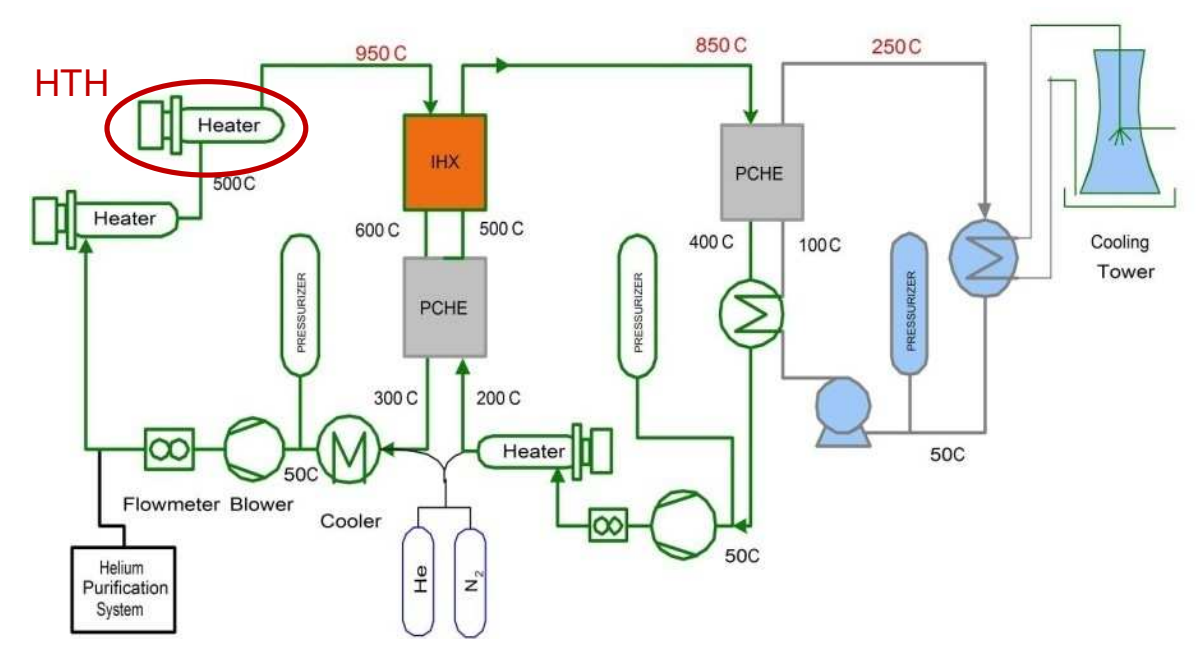


Figure 1 High temperature heater (HTH) in the medium-scale helium loop.

The turbulence intensity at the inlet was defined as a ratio of turbulent velocity fluctuation to averaged velocity, and is assumed as 5% in this simulation. The outlet boundary condition was set as a 'zero gradient', which means that the flow was fully developed and the velocity gradients were zero.

#### 1.3 Material Properties

Helium properties such as pressure, viscosity, thermal conductivity, and heat capacity were supplied as look-up tables depending on the temperature and pressure. The thermal conductivity of the pressure vessel made of SUS-304 steel was 19.0 W/mK. A constant thermal conductivity of 26.0 W/mK was used for the heater, which is made of carbon ceramic (C/C) composite. To minimize the lateral heat loss through pressure vessel wall, a ceramic fiber insulator (Kaowool<sup>TM</sup>) was inserted inside the pressure vessel and its effective thermal conductivity was obtained from an empirical correlation as follows without any directional tendency.

$$\lambda_{eff} = 0.0201 + 6.04 \times 10^{-4} T(K). \text{ [W/mK]}$$
 (15)

Here, T is a local temperature in Kelvin. The maximum operating temperature of this ceramic faber insulator is 1450 °C.

## 2. Preliminary Results

Fig. 2 shows the design of the high-temperature heater obtained from the previous studies. [8, 9] The selected design has 24 electric heaters inside a 2.5m-long pressurized steel vessel, inside

which is a 42mm-thick coaxial insulating pipe made of ceramic fiber. The helium fluid heats up to 500°C in the first low-temperature heater, flows in the second helium heater, and is reheated up to 1000°C before exiting the outlet at a pressure of 9MPa. During this heating process, part of the heat is transferred in the lateral direction and lost to the atmosphere outside the pressure vessel. Due to these high-temperature characteristics, radiation heat transfer also plays an important role in this problem.

As shown in Fig. 2(c), a coarse structured mesh was used in this trial simulation. The standard k- $\varepsilon$  turbulence model was adopted associated with logarithmic wall function due to its efficiency and robustness. To satisfy the requirement of the wall function in the fluid domain, finer grids were inserted near the walls so that the  $y^+$  values inside surfaces of the channel are ranged in 5.0 to 11.0. In the ANSYS CFX code,  $y^+$  values less than 11.06 are automatically scaled up to 11.06. The P-1 radiation heat transfer model was applied to estimate the radiational heat transfer from the heater surfaces to the inner wall of the insulator (actually reflector's inner surface). 251 uniform nodes in the axial direction were placed, so the total number of nodes becomes 4,056,918. Thermal-fluidic analyses with total heat loads of 270 - 300kW and a mass flow rate of

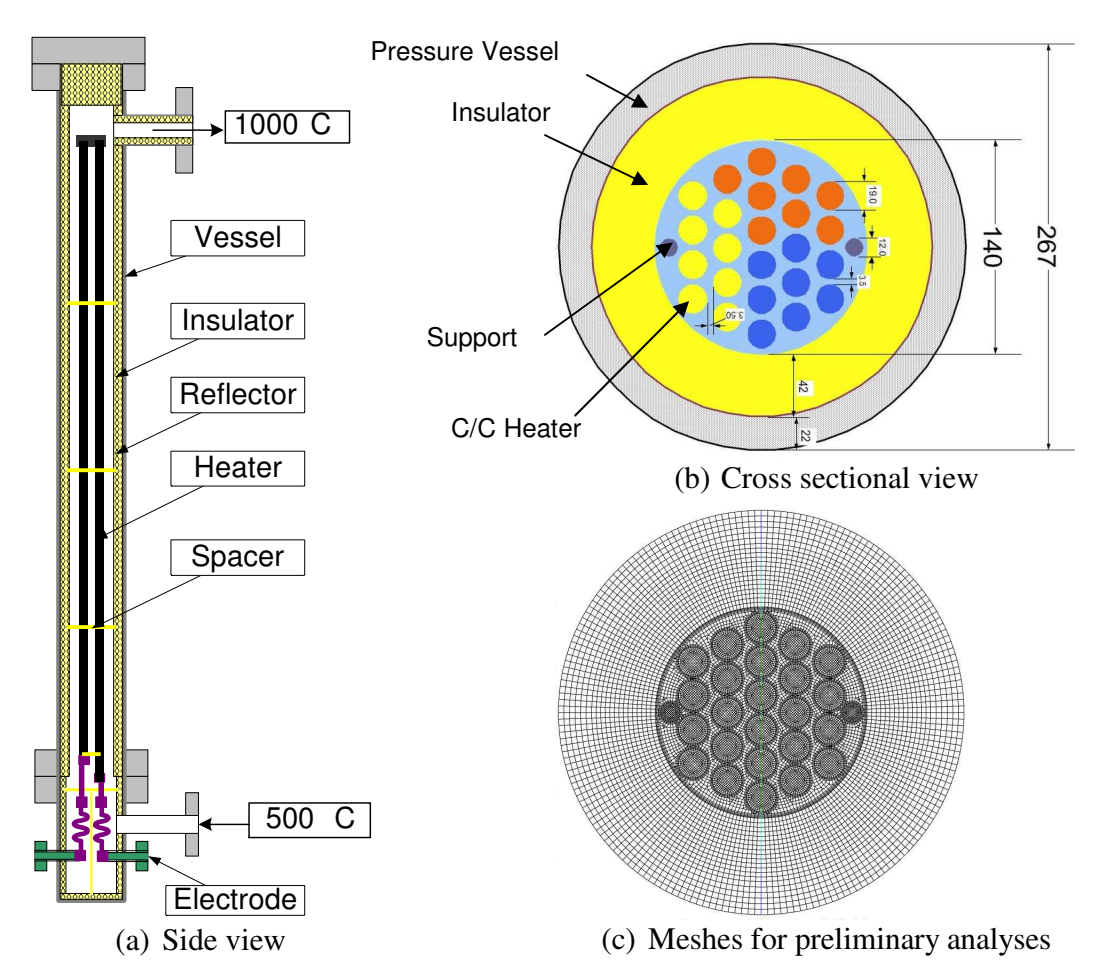


Figure 2 Design of the high-temperature heater

Head Load [kW]	Pressure [MPa]	Flow	Global max. T [°C]	Outlet average T [°C]	Outer surface min. T [°C]	Outer surface max. T [°C]	Max. axial velocity [m/s]
	9	Turb.	1170.98	962.75	158.99	287.92	4.38
270	9	Lam.	1316.95	963.74	160.35	335.05	6.40
270	1	Turb.	1168.86	958.68	159.39	287.02	39.24
		Lam.	1312.98	959.77	160.61	334.42	57.47
	9	Turb.	1237.23	1014.09	163.80	305.90	4.54
200	9	Lam.	1394.65	1014.95	164.93	354.83	6.62
300	1	Turb.	1233.50	1009.57	164.30	304.82	40.75
	1	Lam.	1391.78	1010.52	165.22	354.11	59.56

Table 2 Temperature and velocity parameters of preliminary analyses

0.1 kg/s at 1 MPa and 9 MPa were performed. The total heat load was assumed to be uniform over the 24 heat rods assuming homogeneous material composition and constant cross-sectional areas along the axis, and the inlet velocities were also set to be uniform neglecting the complex inlet and outlet geometric effects in this study. To obtain conservative results, laminar flow simulations were also conducted since the Reynolds number was low even in the turbulence region. These steady state parallel computations using ANSYS CFX-13.1 were performed on INTEL Xeon processors. The convergence criterion was the root mean square (RMS) residual of  $10^{-6}$  and the largest energy imbalance of 0.01%.

Figure 3 shows the results of a turbulent analysis with 270 kW heat load at 9 MPa. The maximum temperature of 1,171 °C was found in the central heater near the exit. The outer surface temperatures of the pressure vessel were in the range of 159 °C to 288 °C. The maximum axial velocity was about 4.4 m/s. Table 2 summarizes the resultant temperature and velocity values for each case.

From the preliminary simulations, it is confirmed that the maximum heater temperature would not exceed the maximum allowable temperature of 1600 °C with a temperature margin of more than 300 °C under normal operating conditions. From these preliminary results, the inlet boundary condition would be extracted for the later simulation with more detailed geometry and models.

# 3. Sensitivity of the Separate Effects

In the preliminary simulation, Buoyancy forces were not accounted for and the emissivity value of the reflector (inner surface of the insulator) was set to be 1.0. In this chapter, Buoyancy forces

are included for vertical or horizontal heater installations and a various values of the reflector's emissivity are tested to select the reflector material among candidates.

For this sensitivity studies, the standard k- $\varepsilon$  model associated with the scalable wall function and the P-I radiation heat transfer model were adopted on the same meshes used in the preliminary analyses.

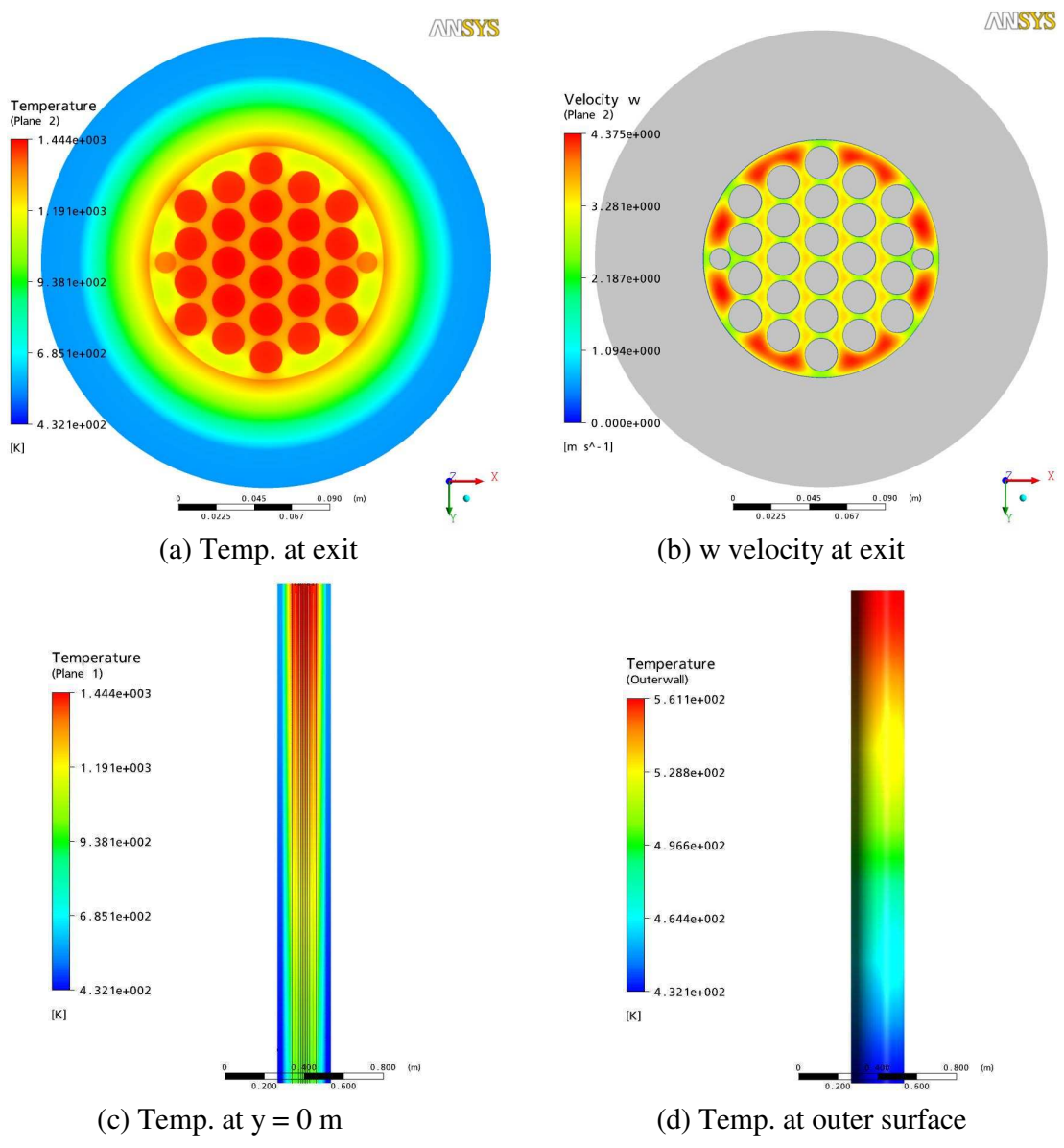
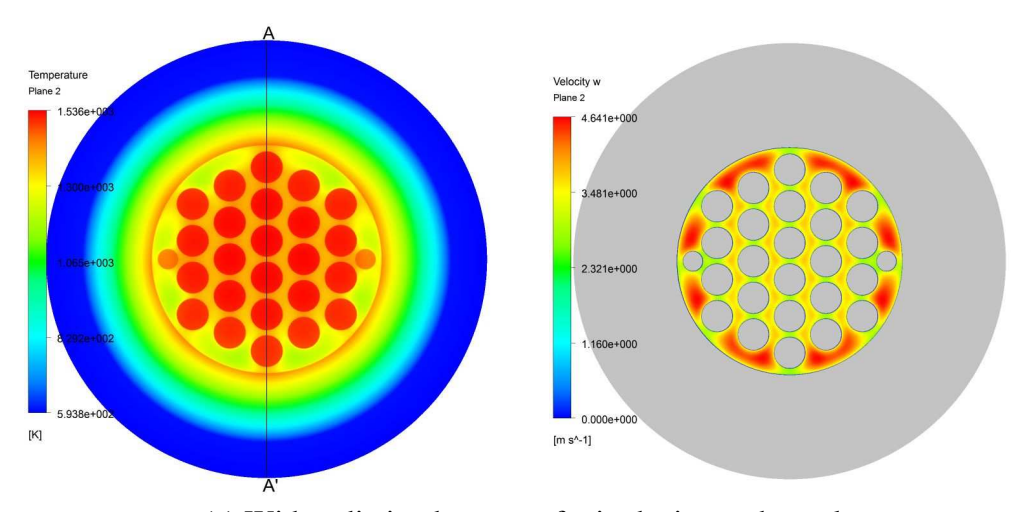


Figure 3 Preliminary results with radiation calculation: 300 kW heat load, P = 9 MPa,  $k-\varepsilon$  turbulence model, P-1 radiation model

## 3.1 Buoyancy Effects

Helium is an ideal gas, and in a fluid is basically Buoyant under heating processes. To examine its Buoyancy effects, analyses were performed accounting for the gravitational forces assuming horizontal or vertical installations of the heater. The base used for the comparison was the results of a turbulent analysis with a 300 kW heat load at 9 MPa.

In a horizontal installation of the heater, a gravitational force of  $9.80665 \text{ m/s}^2$  works in the -Y direction of the applied coordinate system. An example of horizontally-installed helium heaters for a VHTR experimental studies can be found in the Helium Test Facility (HTF) of Pebble Bed Modular Reactor (PBMR) Ltd. Figure 4(a) shows the analysis results accounting for the gravitational force, which show no significant changes from the base level. However, the anticipated Buoyancy effect appears clearly in Fig. 4(b) when we remove the radiation heat



(a) With radiation heat transfer in the inner channel

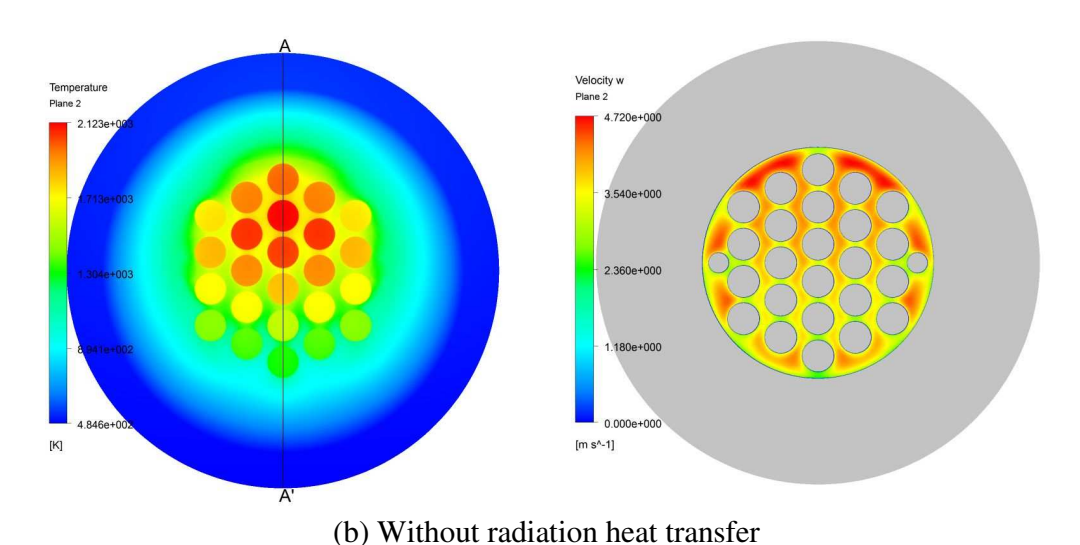


Figure 4 Results with gravitation in the –Y direction: Horizontal installation of the heater.

Table 3 Outlet helium temperature and W velocity component for a vertical installation of HTH

	Vertically Upward	Base Case	Vertically Downward
Outlet massflow-averaged Temperature [°C]	1049.42	1014.09	1049.41
Outlet area-averaged W velocity [m/s]	3.64067	3.53908	3.64069

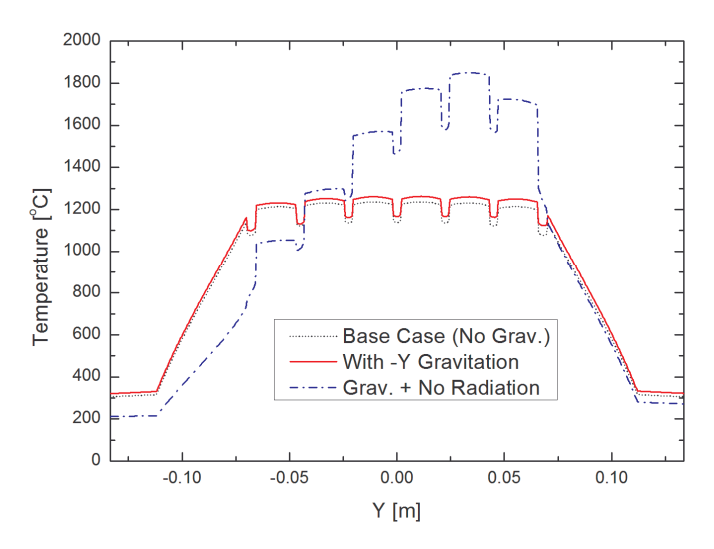


Figure 5 Vertical temperature profiles at the exit (Z = 2.49m) for a horizontal installation of the HTH: gravity effect.

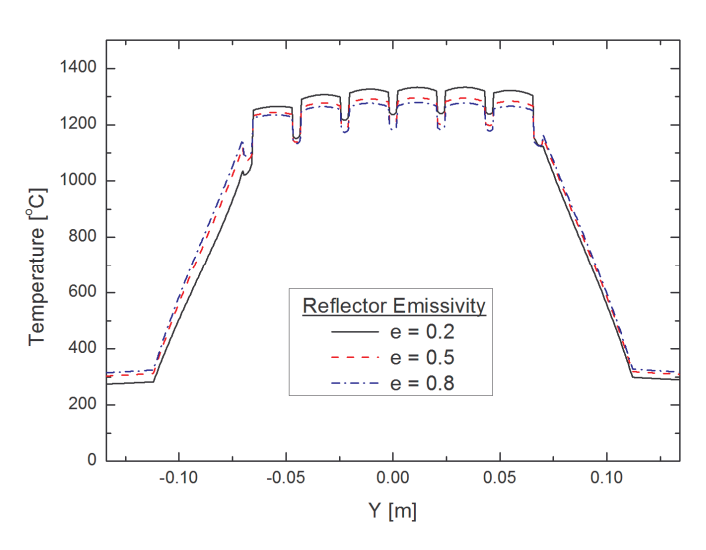


Figure 6 Vertical temperature profiles at the exit (Z = 2.49m) for a horizontal installation of the HTH: Sensitivity of the reflector emissivity with gravity.

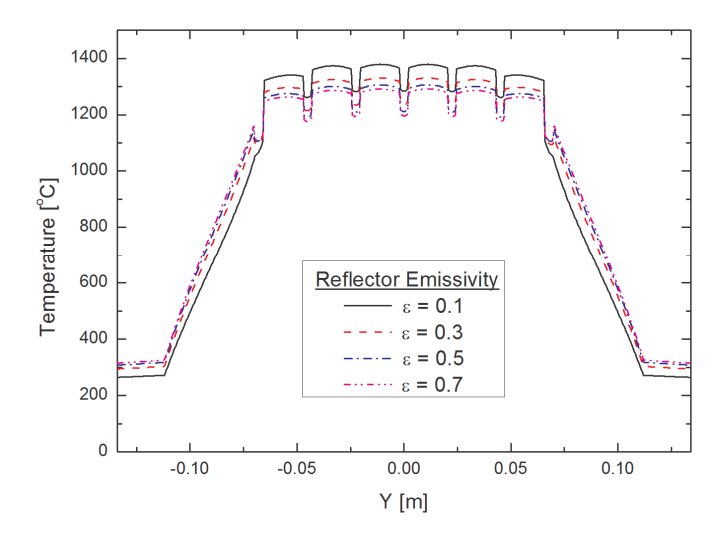


Figure 7 Vertical temperature profiles at the exit (Z = 2.49m): Sensitivity of the reflector emissivity without gravity.

transfer from the analysis model. The temperature profiles in the A-A' line are compared in Fig. 5. The temperature profiles of the base case and current results are similar except that the current results show a higher maximum temperature of about 4 °C. Also, local temperatures in the upper region (+Y region) increase when we apply gravitation in the -Y direction without a radiation heat transfer inside the Helium channel.

As a result, we concluded that there should not be any severe local temperature increases in a horizontally-installed helium heater because the radiation-heated inner surfaces of the channel suppressed the Buoyancy forces.

In a vertical installation of the heater, there was no significant disturbance in fluid temperature or velocity. Table 3 summarizes the temperature and velocity changes for a vertical installation. Slight increases in velocities were thought to be caused by density changes according to the temperature increases.

To avoid possible flow disturbance due to gravitation during some abnormal operating conditions such as starting-up when the radiative heat transfer will be not fully engaged, a vertical installation of the high temperature heater was decided for the medium scale helium loop in KAERI.

## 3.2 Emissivity of the Reflector

A reflector will be attached to the inside surface of the insulator pipe for controlling the radiation heat transfer in a fluid channel. While the thickness of the reflector was neglected in the conduction heat transfer due to its relatively high conductivity, the emissivity of the reflector was not ignorable and therefore considered in the radiation heat transfer. The emissivity of the electric heaters was assumed to be 0.8, and that of the reflector was set in a range of 0.1 to 0.9. Figures 6 and 7 compare the temperature profiles at the A-A' line near the outlet for various

emissivity levels with and without gravity, respectively. Without gravity, the maximum temperature increases and the reflector temperature decreases as the emissivity of the reflector is lowered. With gravity, the vertical temperature profiles tilt more toward the lower reflector emissivity, but the local temperature changes are bearable.

As a result, Molybdenum was selected for the reflector material, of which the emissivity is about 0.2. This low emissivity value reduces heat losses in the lateral direction, and so more heat will be transferred into the coolant. Note that the melting point of high-performance Molybdenum is around  $1850\,^{\circ}$ C, and that oxides of Molybdenum have the emissivity values of  $0.80\,\sim0.84$ .

# 4. Detailed Simulation with Spacers

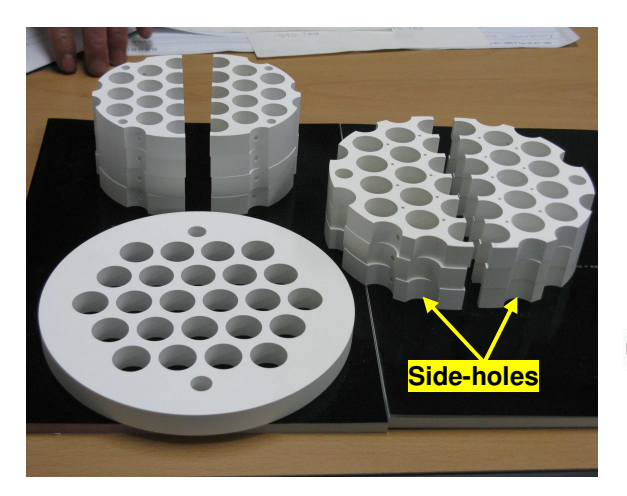
More detailed analyses on the HTH of the medium scale helium loop are described in this chapter. In preliminary analyses, a full length of the 2.5 m heating channel of the HTH was facilitated for a computational domain with a uniform cross-section, where geometric configurations of the heating channel are independent of axial distance. However, the actual design of the heater has five equally-located spacers and two end-mounts to hold the 24 heaters. Each spacer made of 15mm-thick Boron Nitride covers half passage and is installed in staggered arrangement with intervals of 0.5 m. Figure 8 shows three kinds of spacers, of which the spacers for the HTH in the right, the end-mounts in the left bottom, and the spacers for other smaller heaters are in the left top.

For the more detailed analyses, a computational domain was set for only downstream part of the HTH including two spacers as shown in Fig. 9. The reason of utilizing a part of geometry is that cell number of the coarse meshes for the preliminary analyses already reached a critical point to seriously reduce computing efficiency. The domain includes two spacers 500mm apart and 250mm extended regions on both upstream and downstream sides, so that total length of the computed channel becomes 1.015 m. The inlet temperature and velocity boundary conditions are extracted from the preliminary analyses results. Thermal-fluidic effects of side holes were examined by comparing the results with and without side holes. To satisfy the requirement of the wall function in the fluid domain, finer grids were inserted near the walls to give the y<sup>+</sup> values less than 2.0. 406 uniform nodes in the axial direction were placed, so the total number of nodes becomes about 12.0 million. Figure 10 shows a cross-sectional view of meshes and the inlet temperature boundary condition. In this simulation it is assumed that the HTH were vertically installed, and that the emissivity of the reflector surface was set as 0.2.

The continuity, momentum, and energy equations associated with the transport equations of turbulent kinetic energy and specific dissipation rate were solved for the fluid domain by using a commercial CFD code, ANSYS CFX release 12.0. The shear-stress transport (SST) k- $\omega$  turbulence model with the discrete transfer (DT) radiation model was adopted in the detailed analyses. These steady state parallel computations using ANSYS CFX-13.1 were performed on INTEL Xeon processors. The convergence criterion was the root mean square (RMS) residual of  $10^{-6}$  and the largest energy imbalance of 0.01%.

Tables 4 and 5 summarize the resultant temperature and velocity parameters for the case of spacers with and without side-holes, respectively. Due to the installation of spacers occupying about the half of the fluid passage, the maximum fluid velocity increased up to about twice that of the preliminary analyses results without spacers. The local heater temperature increased at the spacer locations by about 50 °C compared to those of the preliminary results. Compared to the case of spacers without side-holes, the global maximum temperature, the maximum temperature of vessel outer surface, and the global helium maximum velocity decreases by about 8.6°C, about 30°C, and 1.7 m/s for the spacers with side-holes, respectively.

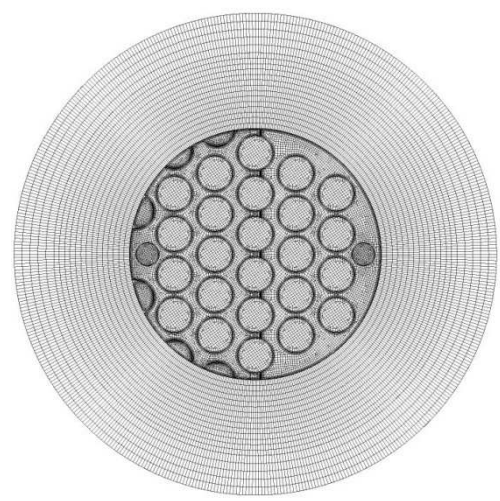
Figure 11 shows the stream lines colored by fluid velocity magnitude for the case of spacers with and without side-holes. It is thought that the improvements in thermal-fluidic performances by side-holes were due to washout of the recirculation by the fluid flows through side-holes.

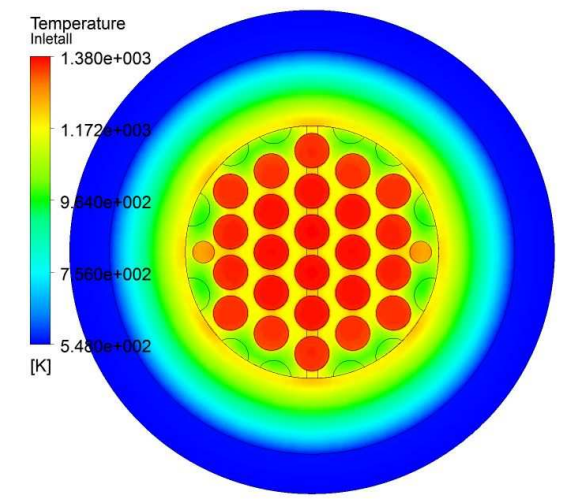


Spacers

Figure 8 Spacers (Boron Nitride)

Figure 9 Computational domain for detailed calculation





(a) Meshes at cross section

(b) Temperature distributions at inlet

Figure 10 Meshes and inlet temperature boundary condition

Table 4 Temperature and velocity parameters for the case of spacers without side-holes

Head Load [kW]	Turbulence Model	Radiation Model	Global max. T [°C]	Outlet average T [°C]	Outer surface max. T [°C]	Max. axial velocity [m/s]
	$k extcolor{black}{arepsilon}$	P-1	1270.1	1007.6	300.4	10.0
270	SST	P-1	1221.2	1010.8	293.2	11.7
270	SST	DT	1413.8	1012.4	304. 5	11.8
	Average		1301.7 ± 112	$1010.3 \pm 2.7$	$299.3 \pm 6.2$	11.17 ± 1.2
	$k extcolor{black}{arepsilon}$	P-1	1338.5	1064.2	317.5	10.4
	SST	P-1	1285.3	1067.5	308.5	12.2
300	SST	DT	1513.3	1069.8	321.1	12.2
	Average		1379.0 ± 134.3	$1067.2 \pm 3.0$	$315.7 \pm 7.2$	11.6 ± 1.2

Table 5 Temperature and velocity parameters for the case of spacers with side-holes

Head Load [kW]	Turbulence Model	Radiation Model	Global max. T [°C]	Outlet average T [°C]	Outer surface max. T [°C]	Max. axial velocity [m/s]
	k-€	P-1	1211.4	1008.0	270.9	8.6
270	SST	P-1	1181.2	1012.7	269.2	9.9
270	SST	DT	1276.5	1013.8	261.4	10.9
	Average		1223.0 ±53.5	$1011.5 \pm 3.5$	$267.2 \pm 5.8$	$9.8 \pm 1.2$
	k-€	P-1	1281.7	1065.2	287.3	9.0
300	SST	P-1	1252.6	1068.9	283.8	10.3
	SST	DT	1354.7	1071.8	279.3	11.3
	Ave	rage	1296.3 ±58.4	$1068.6 \pm 3.4$	$283.5 \pm 4.2$	10.2 ± 1.2

Figure 12 shows the temperature distributions and velocity fields of some interested locations for a detailed analysis with 270 kW heat load at a pressure of 9 MPa. Note that the temperature bands at the outer surface of the pressure vessel skewed due to the existence of spacers.

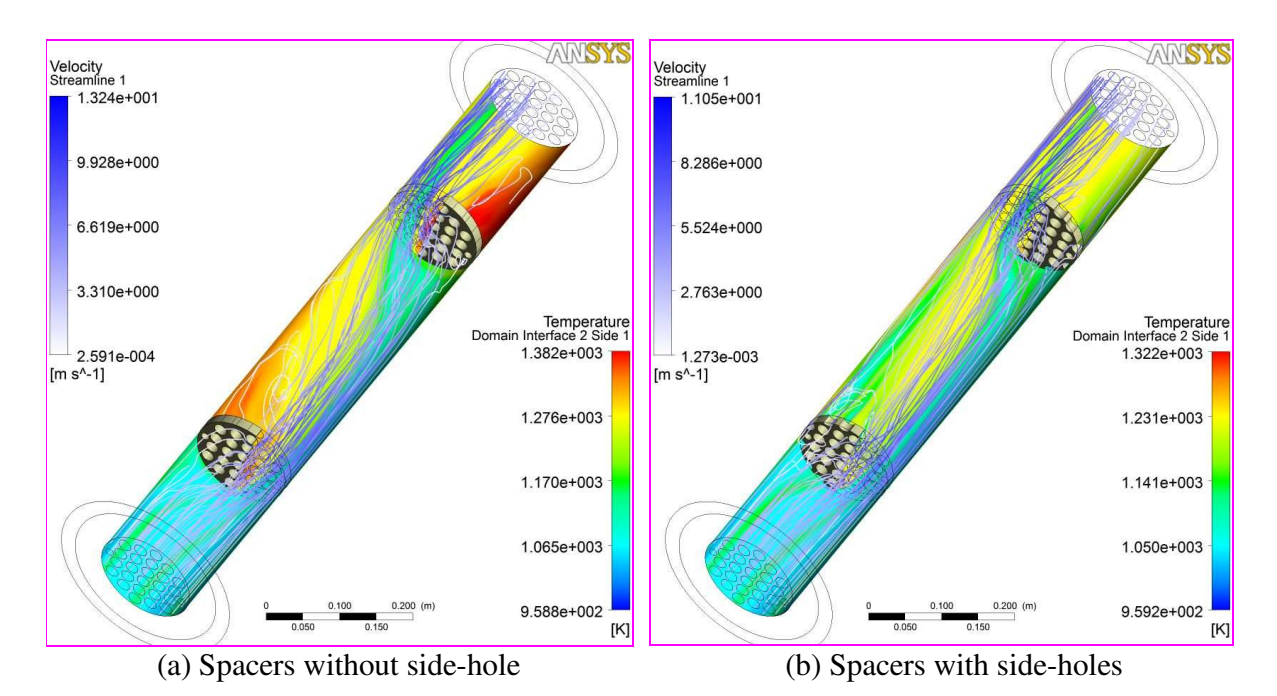
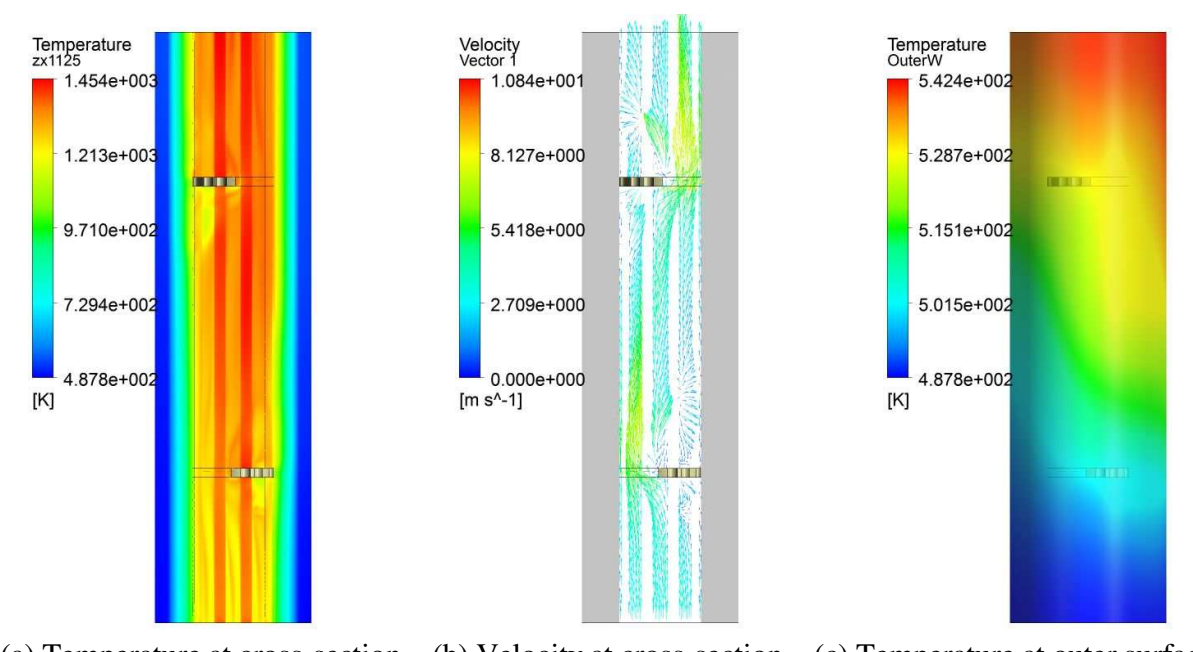


Figure 11 Side-hole effects: 270 kW heat load, P = 9 MPa, SST turbulence model, P-1 radiation model



(a) Temperature at cross-section (b) Velocity at cross-section (c) Temperature at outer surface Figure 12 Results at side views: 270 kW heat load, P = 9 MPa, *SST* turbulence model, *DT* radiation model.

# 5. Grid Sensitivity

Grid refinement studies in the current CFD simulation are performed by using 4 different mesh densities for the cases without spacers as listed in Table 6. Strict quantitative evaluation of grid refinement study [10] was not performed due to the complexity of geometry and the limited computer capability. The shear-stress transport (SST) k- $\omega$  turbulence model with the simple P-I radiation model was adopted for all cases. Due to the limitation of computing capabilities, Case III and IV respectively utilize a short domain and a short and half domain. These grid refinement studies concentrate on the fluid domain rather than solid regions. The grid density of the preliminary analyses is about the same as Case I, and that of the detailed analyses is between Case III and Case IV. The differences of all major parameters between Case III and IV are less than 0.2%, so that it is presumed that the mesh density of the detailed analyses were well in the asymptotic range where the decretization errors are small enough.

Table 6 List of cases for the grid refinement studies

	Case I	Case II	Case III	Case IV		
Geometric domain	Full (2.5m-long)	Full (2.5m-long)	Short (1.015m-long)	Short (1.015m-long) and half		
Number of nodes in fluid region	4,036,056	8,758,983	8,681,717	8,600,922		
Number of total nodes	6,636,918	11,359,845	15,018,707	11,273,691		
Near-wall y <sup>+</sup> value	< 2	< 2	< 2	< 2		
Axial node spacing	5 mm	5 mm	2.5 mm	1.4 mm		
	Analysis Results					
Global maximum temperature [°C]	1332.8	1342.9	1345.2	1347.9		
Outlet average temperature [°C]	1057.6	1056.4	1067.0	1067.7		
Maximum outer surface temperature [°C]	275.2	304.9	280.8	281.2		
Global maximum velocity [m/s]	5.7533	5.4682 5.2535		5.2545		

#### 6. Conclusions

In this study, the thermal-fluidic behaviours of a candidate design of the HTH (High-temperature heater) were analysed by using CFD technique. Due to the large temperature differences in the domain, radiation heat transfer was not ignorable. The major findings are as follows:

- Due to the large temperature difference, radiation heat transfer is essential in the analysis. By radiation heat transfer, the insulator inner surface becomes hotter than the near-wall helium fluid.
- The hotter inner surface suppresses Buoyancy forces induced by gravity, which are expected in the case of horizontal installation.
- A sensitivity study of the reflector's emissivity was performed for assuring the selection of Molybdenum liner.
- Installation of the spacers with side-holes increases the flow velocities and turbulent intensities, and decreases the outer surface temperature. Therefore, the thermal-fluidic characteristics of the HTH improve, even though the local temperatures go up a couple of degree Celsius due to the flow obstacles.
- The mesh densities of the detailed analyses are presumed to be in the asymptotic range.

Finally, it has been confirmed that the thermal-fluidic characteristics of the HTH satisfied the design requirements.

## Acknowledgment

The present study was supported by Nuclear Research & Development Program of the KOSEF grant funded by the MEST of the Korean government.

#### References

- [1] Chang, J. H., et al., "A Study of a Nuclear Hydrogen Production Demonstration Plant," Nuclear Engineering and Technology, Vol. 39, No. 2, 2007, pp. 111~122.
- [2] Bischoff, B. L., et al., "Production of Hydrogen Using Nuclear Energy and Inorganic Membranes," <u>Proceedings of ICAPP'04</u>, Pittsburg, USA, 2004, pp. 2137~2145.
- [3] Hong, S. D., et al., "Design of a Small Scale High Temperature Gas Loop for Developing a Process Heat Exchanger of Nuclear Hydrogen Production Module," <u>KSME Spring Meeting</u>, ROK, pp. 2067~2072.
- [4] Hong, S. D., et al., "Development of a Compact Nuclear Hydrogen Coupled Components Test Loop," KSME Autumn Meeting, ROK, 2008, pp. 2850~2855.

- [5] Kim, Y.W., et al., "A High Temperature Gas Loop to Simulate VHTR and Nuclear Hydrogen Production System," <u>20th Int. Conference on Structural Mechanics in Reactor Technology</u> (SMiRT 20), Finland, Paper 1870, 2009.
- [6] CFX-11.0: Solver Theory, 2008, ANSYS Canada Ltd., Canada. (Web form)
- [7] M. F. Modest, *Radiative Heat Transfer*, Int'l Ed., McGraw-Hill Inc., 1993.
- [8] Yoon, C., et al., "A CFD Analysis for Designing the VHTR Simulated Experimental Loop," <u>Transactions of the KSME (B)</u>, Vol. 34, No. 5, pp. 553~561.
- [9] Hong, S. D., et al., "The Design and Analytical Validation of a C/C Composite Helium Heater for a VHTR Simulated Experimental Loop," KNS Autumn Meeting, Gyeongju, ROK, 2009, pp. 103~104.
- [10] P. J. Roache, "Perspective: A Method for Uniform Reporting of Grid Refinement Studies," <u>Journal of Fluids Engineering</u>, 116, 405-413, Sep. 1994.

#### **Nomenclature**

$A$ $K_a$ $K_s$ $H$ $I_b$ $I_v$ $S$ $S$ $S$ $T$ $U$ $U_{\tau}$ $X$ $Y^+$ $V$	linear anisotropic coefficient absorption coefficient scattering coefficient enthalpy blackbody emission intensity spectral radiation intensity source path length [m ] directional vector local temperature [K] velocity component [m/sec] friction velocity [m/s] location [m] dimensionless distance from wall [ ] frequency [/s]	$\mu$ $\rho$ $\tau_{w}$ $\Omega$ $\Phi$ b e $w$ $\infty$ $\nu$ r t	dynamic viscosity [kg/sec/m] density [kg/m³] wall shear stress [kg/m/s²] solid angle [sr] in-scattering phase function  Subscripts blackbody or buoyancy effective wall environmental frequency radiational turbulent
--	--	--	---